Understanding benzyl alcohol aggregation by chiral modification: The pairing step

-

Electronic Supplementary Information

Robert Medel and Martin A. Suhm*

Contents

*Institute of Physical Chemistry, University of Goettingen, Tammannstr. 6, 37077 Goettingen. Germany. E-mail: msuhm@gwdg.de

1 Gaussian keywords used in calculations

Table S1: Gaussian[1] keywords used in calculations.

type of calculation	keywords
all	integral(grid=ultrafinegrid)
monomer optimization	opt=verytight
dimer optimization	opt=tight
frequencies with IR and Raman act.	freq=raman
frequencies with only IR act.	freq
transition state optimization	opt=(ts,calcfc,noeigen,tight)
coordinate scan	opt=modredundant
def2-TZVP basis set	def2tzvp
may-cc-pVTZ basis set	may-cc-pvtz
B3LYP-D3(BJ)	b3lyp, empiricaldispersion=gd3bj
M06-2X	m062x
ωB97X-D	wb97xd
B2PLYP-D3(BJ)	b2plyp3

2 Calculation of Raman cross sections

In a first step the Raman activities A_R and depolarisation ratios P from the Gaussian 09 output are converted into the derivatives of the isotropic and anisotropic polarisability α' and γ' according to Eq. 1 and 2.[2]

$$\alpha'^2 = \frac{A_\mathrm{R}}{45}\left(1 - \frac{7P}{3P+3}\right) \tag{1}$$

$$\gamma'^2 = \frac{A_\mathrm{R}P}{3P+3} \tag{2}$$

Detection sensitivity for differently polarised light is accounted for by the empirically determined polynomial in Eq. 3 (by M. Gawrilow, see Ref. 3 for a published variant). For the wavenumbers of the vibrational transitions $\tilde{\nu}$ either the assigned experimental values are used (for calculation of conformational temperatures) or shifted harmonic values (for simulation of spectra).

$$\begin{aligned} f(\tilde{\nu}) = 1.48 &+ 7.2138 \cdot 10^{-10}\tilde{\nu}^3\mathrm{cm}^3 - 7.9373 \cdot 10^{-13}\tilde{\nu}^4\mathrm{cm}^4 \\ &+ 2.7716 \cdot 10^{-16}\tilde{\nu}^5\mathrm{cm}^5 - 0.2071 \cdot 10^{-22}\tilde{\nu}^7\mathrm{cm}^7 \\ &+ 0.4414 \cdot 10^{-26}\tilde{\nu}^8\mathrm{cm}^8 - 2.8952 \cdot 10^{-31}\tilde{\nu}^9\mathrm{cm}^9 \end{aligned} \tag{3}$$

Raman cross sections $\sigma(\tilde{\nu})$ are finally obtained by Eq. 4, using the laser wavelength $\lambda_\mathrm{Laser} = 532.27$ nm and an assumed vibrational temperature $T_\mathrm{v} = 100\,\mathrm{K}$.[4,5] The value of the latter is of little importance for high energetic vibrations, such as OH stretching modes.

$$\sigma(\tilde{\nu}) = \frac{2\pi^2 h \lambda_\mathrm{Laser}^{-1}}{45c} \cdot \frac{\left(\lambda_\mathrm{Laser}^{-1} - \tilde{\nu}\right)^3}{\tilde{\nu}\left(1 - \exp\left(-\frac{hc\tilde{\nu}}{k_\mathrm{B}T_\mathrm{v}}\right)\right)} \cdot \left(45\alpha'^2 + 4\gamma'^2 + \frac{3\gamma'^2}{f(\tilde{\nu})}\right) \tag{4}$$

3 Computational results

3.1 Monomers

3.1.1 Benzyl alcohol

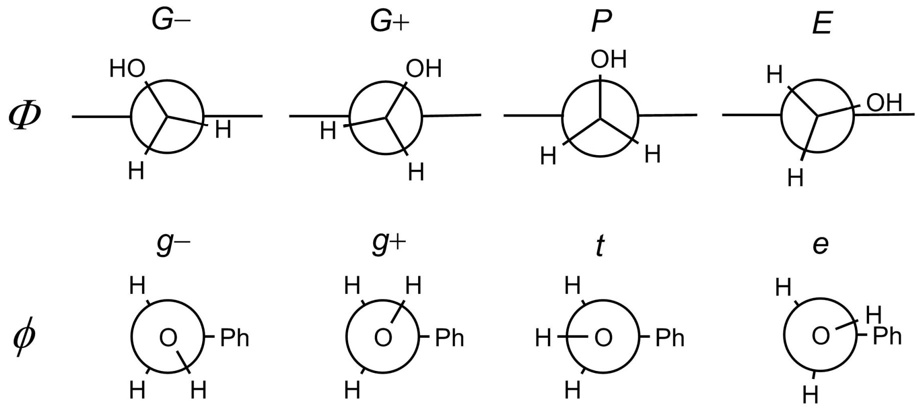

Figure S1: Newman projections along the $C_\alpha{-}C_{ipso}$- (top) and the $O{-}C_\alpha$-bond (bottom) for different sectors of the $OC_\alpha C_{ipso}C_{ortho}$ (Φ) and $HOC_\alpha C_{ipso}$ (ϕ) dihedrals of **B**. G/g means *gauche*, P perpendicular, t *trans* and E/e ecliptic.

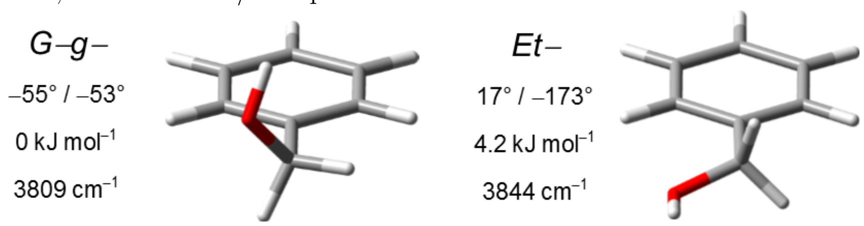

Figure S2: Geometries of the diastereomeric **B** conformers (electronic minima) with the values of the $OC_\alpha C_{ipso}C_{ortho}$ and $HOC_\alpha C_{ipso}$ dihedrals, vibrational zero-point corrected relative energies and harmonic OH stretching wavenumbers at B3LYP-D3/may-cc-pVTZ level.

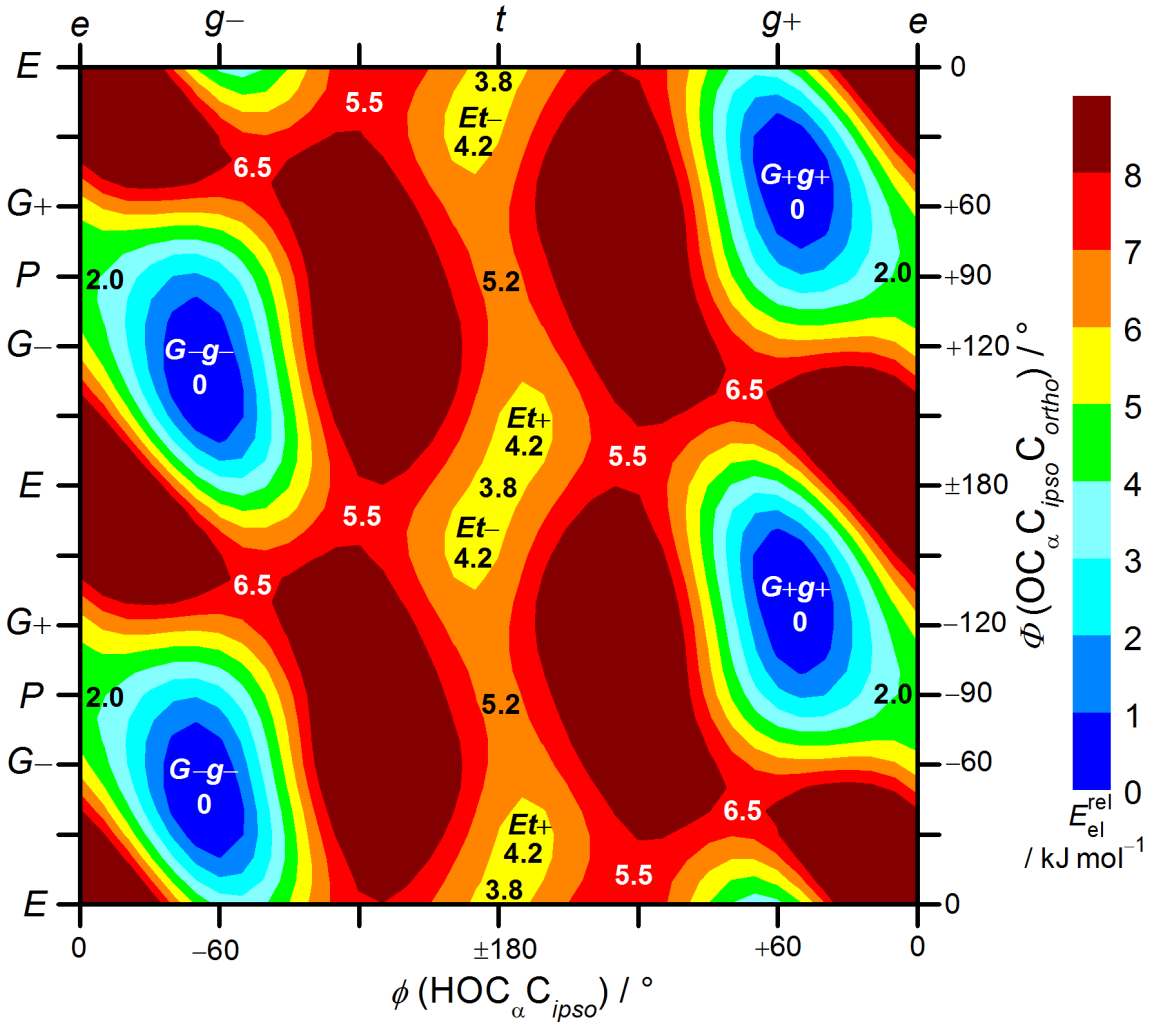

Figure S3: Two-dimensional relaxed scan at B3LYP-D3/def2-TZVP level of the $OC_{\alpha}C_{ipso}C_{ortho}$ (Φ) and the $HOC_{\alpha}C_{ipso}$ (ϕ) dihedral of **B** in 10° steps (1369 data points). Numerical values stated inside the graph represent vibrational zero-point corrected relative energies of minima (labeled) and transition states (unlabeled) after their full reoptimization at B3LYP-D3/may-cc-pVTZ level.

3.1.2 1-Phenylethanol

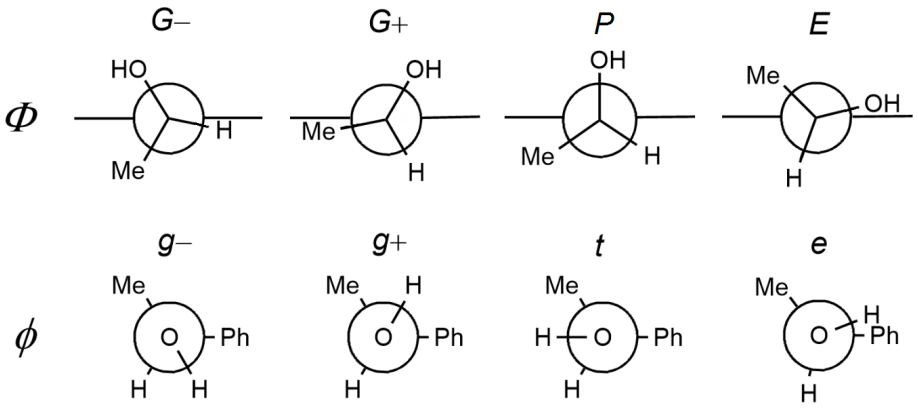

Figure S4: Newman projections along the C_α–C_{ipso}- (top) and the O–C_α-bond (bottom) for different sectors of the $OC_\alpha C_{ipso} C_{ortho}$ (Φ) and $HOC_\alpha C_{ipso}$ (ϕ) dihedrals of (−)-(*S*)-**P**. G/g means *gauche*, P perpendicular, t *trans* and E/e ecliptic.

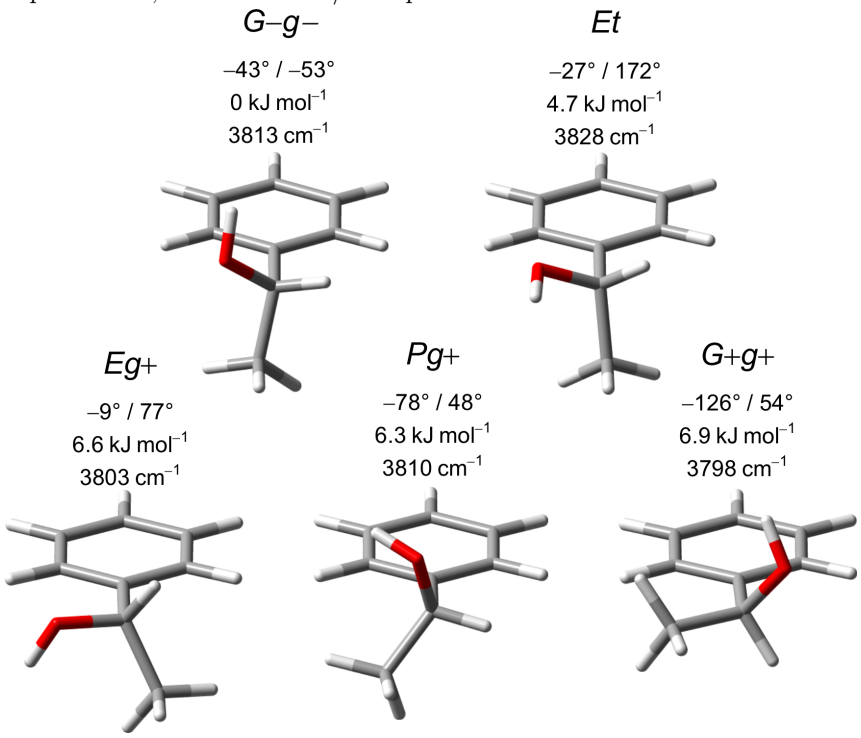

Figure S5: Geometries of the diastereomeric (−)-(*S*)-**P** conformers (electronic minima) with the values of the $OC_\alpha C_{ipso} C_{ortho}$ and $HOC_\alpha C_{ipso}$ dihedrals, vibrational zero-point corrected relative energies and harmonic OH stretching wavenumbers at B3LYP-D3/may-cc-pVTZ level.

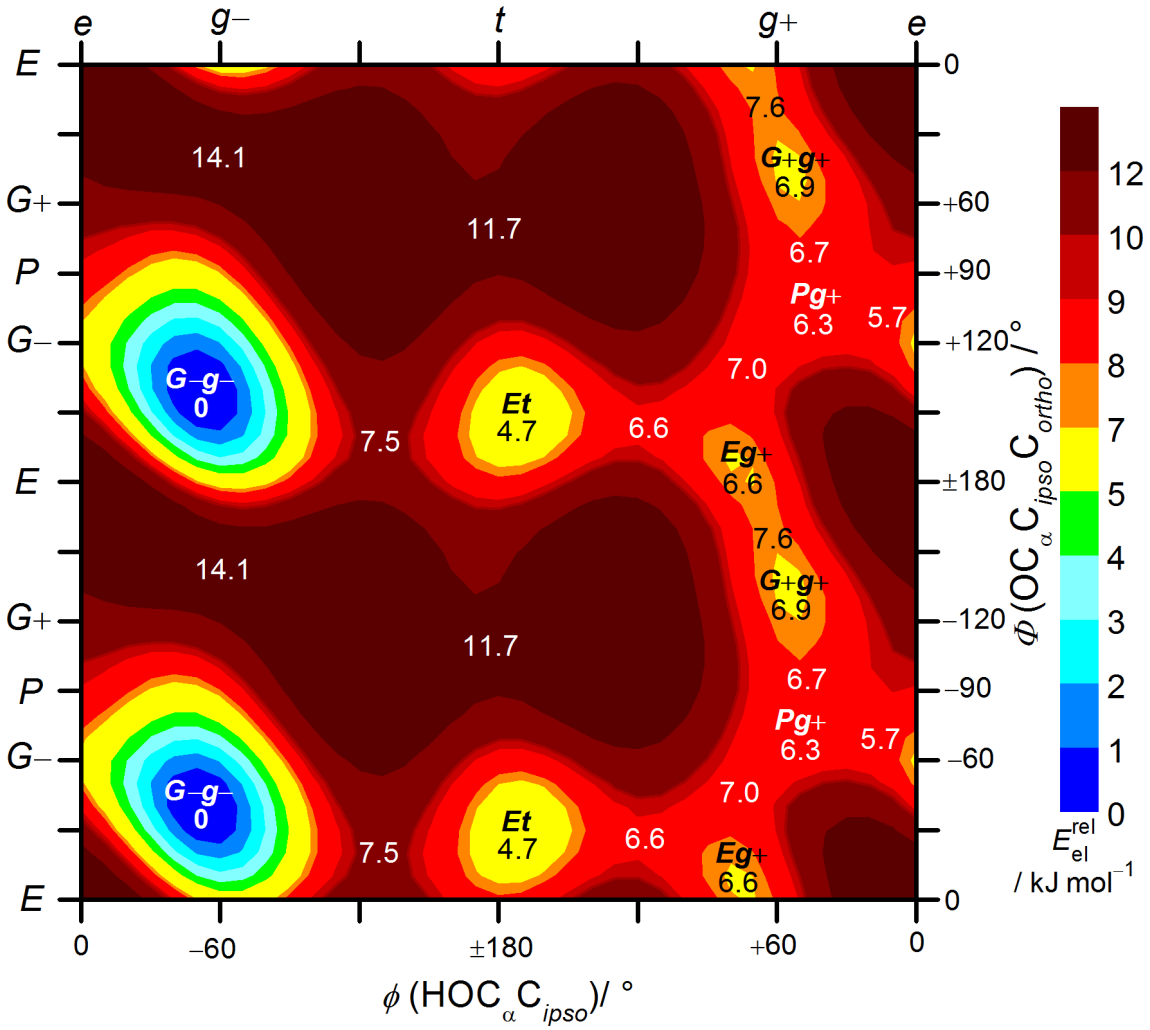

Figure S6: Two-dimensional relaxed scan at B3LYP-D3/def2-TZVP level of the $OC_\alpha C_{ipso} C_{ortho}$ (Φ) and the $HOC_\alpha C_{ipso}$ (ϕ) dihedral of (−)-(*S*)-**P** in 10° steps (1369 data points). Numerical values stated inside the graph represent vibrational zero-point corrected relative energies of minima (labeled) and transition states (unlabeled) after their full reoptimization at B3LYP-D3/may-cc-pVTZ level.

3.2 Dimers

3.2.1 Benzyl alcohol

Table S2: Vibrational zero-point corrected energies of all located **B** dimers at B3LYP-D3/may-cc-pVTZ level. Dimers with two *Gg* monomer conformations are classified as hom or het. Dimers of mixed monomer conformations are classified as *gt* or *tg* according to the $HOC_\alpha C_{ipso}$ dihedrals. Acceptor groups of hydrogen bonds are stated, V means 'vacuum' (= no) acceptor. If different from C_1, the symmetry group is stated. T means a T-shaped orientation of the phenyl rings with respect to each other.

Conformer	E^0_{rel}/ kJ mol^{-1}	Conformer	E^0_{rel}/ kJ mol^{-1}
hom$O^g\pi$	0	*gt* OV	5.2
het$O^g\pi$	0.2	homO^gV T	5.3
het$\pi\pi$ C_i	1.6	het$O^t\pi$ T	5.5
hom$\pi\pi$ C_2	2.0	*gt* OV	7.5
hom$O^t\pi$	3.2	*tg* O^gV	8.4
hetO^gV T	4.3	*gt* Oπ	10.5
homO^gV	4.4	*gt* Oπ	12.1
hetO^gV	4.5	*tg* O^tV	20.8
het$O^t\pi$	4.8		

Table S3: Vibrational zero-point corrected energies of the most important **B** dimers relative to hom$O^g\pi$ in kJ mol^{-1} according to different DFT functionals with may-cc-pVTZ basis set.

	homochiral			heterochiral		
method	$\pi\pi$	$O^g\pi$	$O^t\pi$	$\pi\pi$	$O^g\pi$	$O^t\pi$
B3LYP-D3	2.0	0	3.2	1.6	0.2	4.8
B2PLYP-D3	2.5	0	3.3	2.2	0.1	5.0
ωB97X-D	1.3	0	3.2	−0.04	1.7	4.3
M06-2X	−2.7	0	3.7	−2.2	2.8	3.8

Table S4: Harmonic OH-stretching wavenumbers of the *g*-conformer of **B** and downshifts of **B** dimers in cm^{-1} according to different DFT-functionals with may-cc-pVTZ basis set.

		homochiral			heterochiral		
method	*g*	$\pi\pi$	$O^g\pi$	$O^t\pi$	$\pi\pi$	$O^g\pi$	$O^t\pi$
B3LYP-D3	3809	56/59	53/170	91/158	58/63	68/184	89/145
B2PLYP-D3	3827	55/59	57/163	95/154	56/60	72/177	92/172
ωB97X-D	3895	45/49	54/169	93/143	47/51	72/176	89/139
M06-2X	3875	31/35	59/128	81/113	30/35	66/133	84/114

Table S5: Computed integrated IR band strengths in km/mol for the higher/lower wavenumber OH stretching modes of **B** dimers according to different DFT functionals with may-cc-pVTZ basis set.

	homochiral		heterochiral	
method	ππ	$O^g\pi$	ππ	$O^g\pi$
B3LYP-D3	377/1	124/251	426/0	150/268
B2PLYP-D3	365/0	117/242	409/0	145/256
ωB97X-D	349/7	106/237	373/0	141/249
M06-2X	359/10	141/196	379/0	168/216

Table S6: Computed Raman cross sections in $10^{-36}\,\mathrm{m^2\,sr^{-1}}$ for the higher/lower wavenumber OH stretching modes of **B** dimers according to different DFT functionals with may-cc-pVTZ basis set.

	homochiral		heterochiral	
method	ππ	$O^g\pi$	ππ	$O^g\pi$
B3LYP-D3	1/249	76/81	0/263	84/88
ωB97X-D		58/64	0/198	68/74
M06-2X		53/65	0/172	57/76

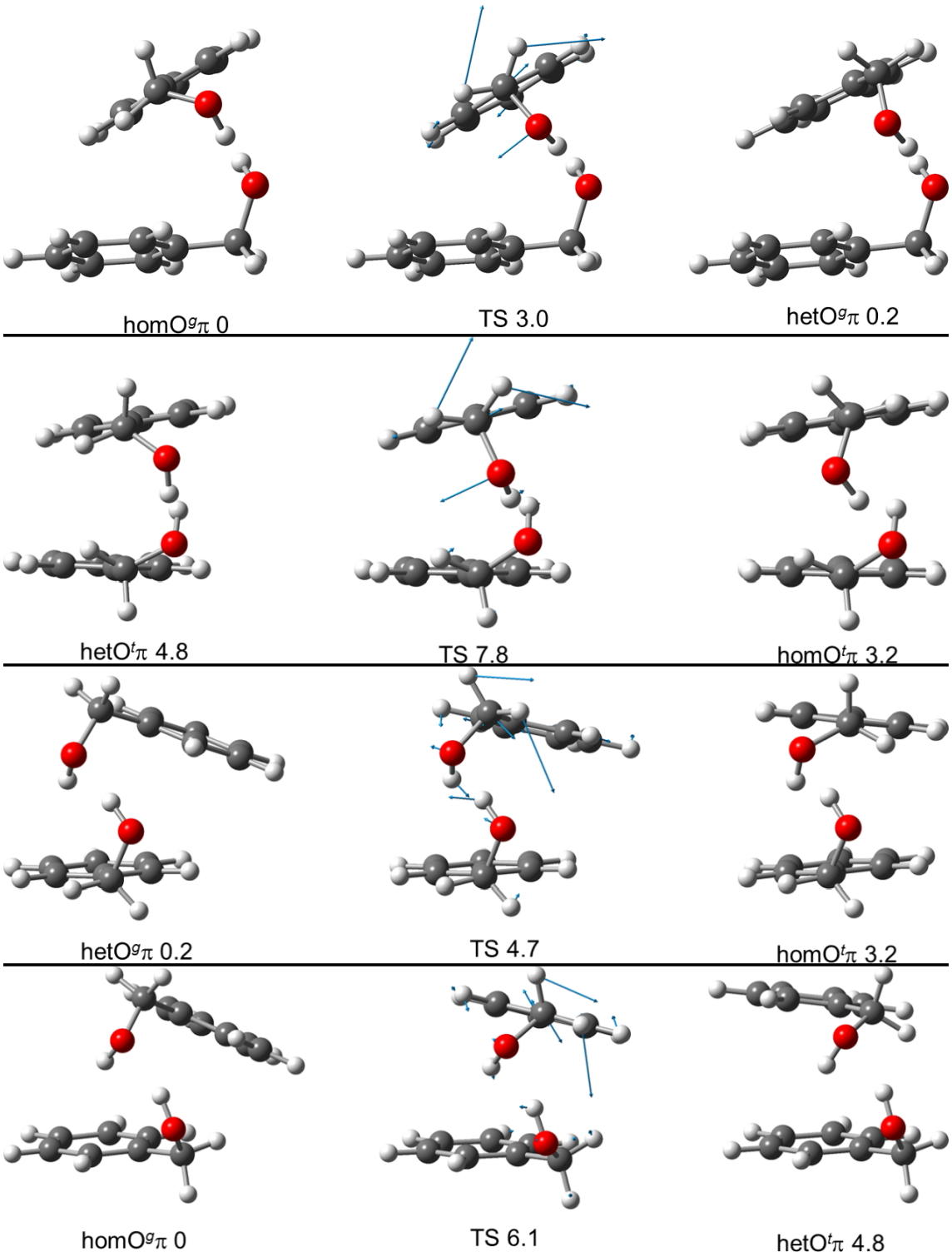

Figure S7: Transition states between **B** dimers at B3LYP-D3 level with respective displacement vectors of the negative curvature coordinate, vibrational zero-point corrected energy in kJ/mol relative to the global minimum and connected minima. Part 1 of 3.

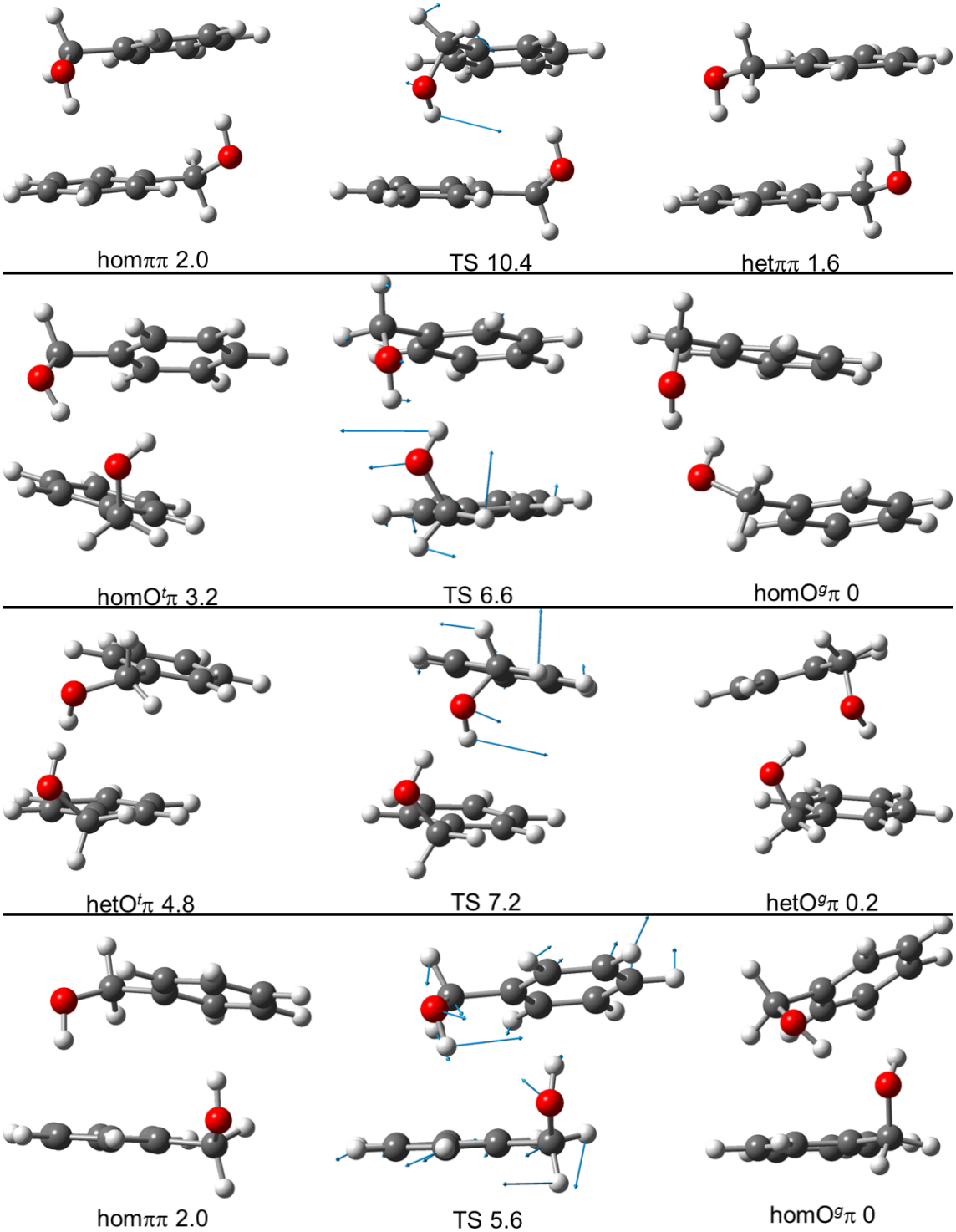

Figure S8: Transition states between **B** dimers at B3LYP-D3 level with respective displacement vectors of the negative curvature coordinate, vibrational zero-point corrected energy in kJ/mol relative to the global minimum and connected minima. Part 2 of 3.

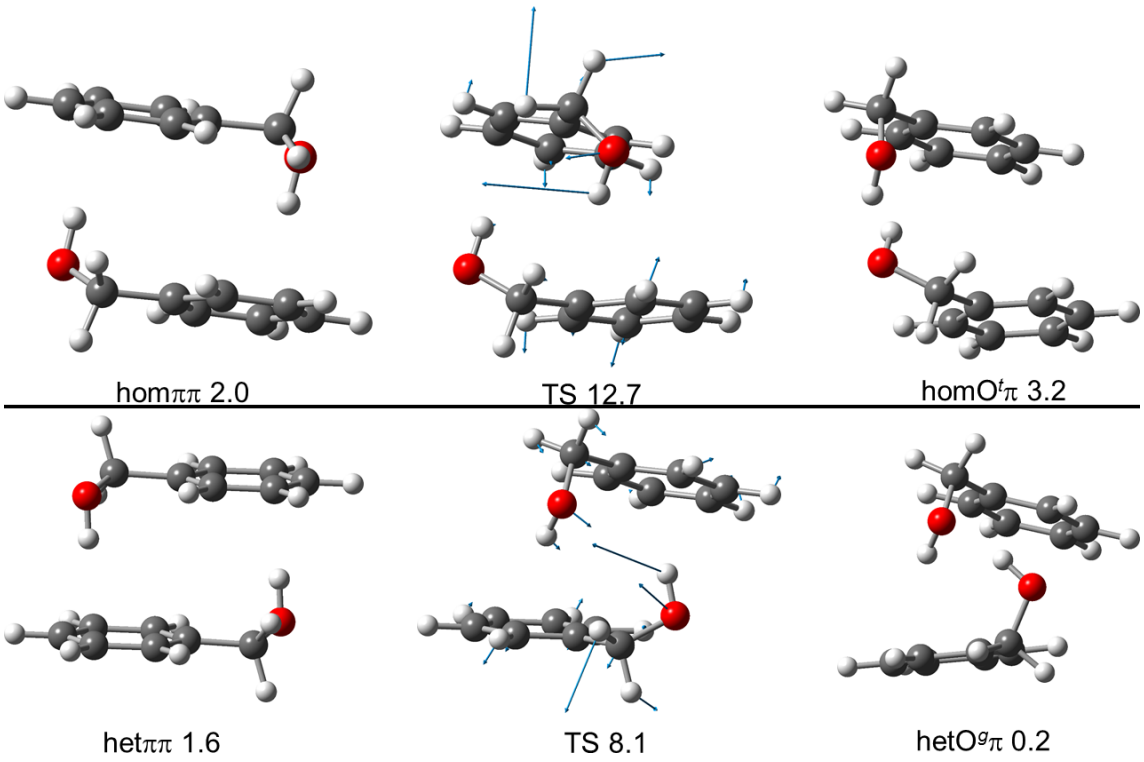

Figure S9: Transition states between **B** dimers at B3LYP-D3 level with respective displacement vectors of the negative curvature coordinate, vibrational zero-point corrected energy in kJ/mol relative to the global minimum and connected minima. Part 3 of 3.

3.2.2 1-Phenylethanol

Table S7: Vibrational zero-point corrected energies of all located **P** dimers at B3LYP-D3/may-cc-pVTZ level, separate for homochiral and heterochiral enantiomer combinations. The heterochiral global minimum is 0.9 kJ/mol above the homochiral one. Monomers with the most stable monomer conformation (common signs of the flexible dihedrals and the optical rotation) are labeled g, otherwise g' or t depending on the $HOC_\alpha C_{ipso}$ dihedral. Acceptor groups of hydrogen bonds are stated, V means 'vacuum' (= no) acceptor. If different from C_1, the symmetry group is stated. T means a T-shaped orientation of the phenyl rings with respect to each other.

hom-Konformer	E^0_{rel}/ kJ mol^{-1}	het-Konformer	E^0_{rel}/ kJ mol^{-1}
gg O$^g\pi$	0	gg O$^g\pi$	0
gg $\pi\pi$ C_2	1.0	gg $\pi\pi$ C_i	1.1
gg O$^t\pi$	1.9	gg O$^t\pi$	1.8
gg O^{g}V T	2.6	gg O^{g}V T	2.3
gg O^{t}V T	4.4	gg' O$^g\pi$	3.3
gg' O$^g\pi$	6.0	gg O^{t}V T	3.9
g'g O$^g\pi$	6.7	g'g O$^t\pi$	6.7
gg O^{g}V	7.0	g'g $\pi\pi$	7.7
g'g $\pi\pi$	7.8	gg' O$^t\pi$	7.9
gg' O$^t\pi$	8.9	gt Oπ	8.4
gt Oπ	9.0	gt Oπ	10.3
g'g O$^t\pi$	9.2	g'g' O$^g\pi$	10.9
gt Oπ	10.9	g'g' $\pi\pi$	14.0
g'g' O$^g\pi$	11.2	g'g' O$^t\pi$	15.4
g'g' $\pi\pi$ C_2	14.2		
g'g' O$^t\pi$	14.7		

Table S8: Vibrational zero-point corrected energies of the most important **P** dimers relative to hom O$^g\pi$ in kJ mol^{-1} according to different DFT-functionals with may-cc-pVTZ basis set.

	homochiral			heterochiral		
method	$\pi\pi$	O$^g\pi$	O$^t\pi$	$\pi\pi$	O$^g\pi$	O$^t\pi$
B3LYP-D3	1.0	0	1.9	2.0	0.9	2.7
B2PLYP-D3	1.1	0	1.9	1.9	0.9	2.6
ωB97X-D	0.9	0	2.7	1.2	2.5	2.9
M06-2X	−2.0	0	2.2	−1.7	2.1	2.0

Table S9: Harmonic OH-stretching wavenumbers of the *g*-conformer of **P** and downshifts of **P** dimers in cm^{-1} according to different DFT-functionals with may-cc-pVTZ basis set.

		homochiral			heterochiral		
method	*g*	$\pi\pi$	O$^g\pi$	O$^t\pi$	$\pi\pi$	O$^g\pi$	O$^t\pi$
B3LYP-D3	3813	52/56	62/164	87/164	58/63	70/177	84/159
B2PLYP-D3	3827	53/57	68/156	92/159	56/61	76/168	89/153
ωB97X-D	3897	42/46	61/164	90/152	51/55	74/174	87/151
M06-2X	3877	41/45	59/121	81/119	30/34	63/130	76/120

Table S10: Computed integrated IR band strengths in km/mol for the higher/lower wavenumber OH stretching modes of **P** dimers according to different DFT functionals with may-cc-pVTZ basis set.

	homochiral		heterochiral	
method	$\pi\pi$	$O^g\pi$	$\pi\pi$	$O^g\pi$
B3LYP-D3	386/2	170/269	478/0	178/297
B2PLYP-D3	373/1	169/249	451/0	178/275
ωB97X-D	336/1	146/254	422/0	166/283
M06-2X	390/8	186/202	408/0	177/239

Table S11: Computed Raman cross sections in $10^{-36}\,m^2\,sr^{-1}$ for the higher/lower wavenumber OH stretching modes of **P** dimers according to different DFT functionals with may-cc-pVTZ basis set.

	homochiral		heterochiral	
method	$\pi\pi$	$O^g\pi$	$\pi\pi$	$O^g\pi$
B3LYP-D3	0/323	114/124	0/375	116/133
ωB97X-D	0/265	88/95	0/231	85/114
M06-2X	13/232	78/101	0/292	79/112

4 Experimental band positions and assignments

Table S12: Experimental band positions and assignments for **B**.

$\tilde{\nu}/\mathrm{cm}^{-1}$	assignment
3648	monomer $G+g+/G-g-$
3598	dimer het$\pi\pi$ (+ hom$\pi\pi$?) antisymmetric
3594	dimer het$\pi\pi$ (+ hom$\pi\pi$?) symmetric
3582	dimer hom$\mathrm{O}^g\pi$ (OH$\cdots\pi$)
3576	dimer het$\mathrm{O}^g\pi$ (OH$\cdots\pi$)
3561	trimer
3555	?
3547	trimer?
3538	trimer?
3514	dimer hom$\mathrm{O}^g\pi$ (OH$\cdots$O)
3504	dimer het$\mathrm{O}^g\pi$ (OH$\cdots$O)
3441	trimer
3433	trimer
3426	trimer
3517	trimer
3374	trimer
3364	?
3347	>trimer
3333	>trimer
3330–3250	>trimer

Table S13: Experimental band positions and assignments for **P**.

$\tilde{\nu}/\mathrm{cm}^{-1}$	assignment
3648	monomer $G+g+/G-g-$
3597	dimer het$\pi\pi$ antisymmetric
3592	dimer het$\pi\pi$ symmetric
3592	dimer hom$\pi\pi$ symmetric
3575	dimer hom$\mathrm{O}^g\pi$ (OH$\cdots\pi$)
3573	dimer het$\mathrm{O}^g\pi$ (OH$\cdots\pi$)
3568	? hom
3564	? hom
3559	? het
3557	trimer? hom
3552	? het
3545	? hom
3540	? het
3516	dimer hom$\mathrm{O}^g\pi$ (OH$\cdots$O)
3514	dimer het$\mathrm{O}^t\pi$ (OH$\cdots$O)?
3507	dimer hom$\mathrm{O}^t\pi$ (OH$\cdots$O)?
3506	dimer het$\mathrm{O}^g\pi$ (OH$\cdots$O)
3440	trimer? het
3417	trimer? hom
3403	trimer? het
3378	trimer? hom
3369	trimer? het
3356	trimer? hom
3349	trimer? het
3274	tetramer? hom

5 Experimental band integral ratios

Table S14: Mean, 2.5% and 97.5% quantile of experimental integral ratios as well as integration widths for different band pairs from 100 000 Monte Carlo evaluations.[6] To account for the partial band overlap in the **B** case, the mean integration width was adjusted for each band pair integration, especially with involvement of the band at 3576cm^{-1}. This additional uncertainty is reflected in a broader distribution of obtained band ratios. Reasonability of results was checked by visual inspection of sample integration areas and by comparison with results from manual integration.

spectrum	band positions / cm^{-1}	2.5% quantile	mean	97.5% quantile	integration width / cm^{-1}
B IR	3514/3582	1.16	1.26	1.36	4±0.4
B IR	3504/3576	1.39	3.6	11.1	3±0.3
B IR	3514/3504	5.1	7.2	11.0	5±0.5
B IR	3582/3576	9.3	12.4	67	3±0.3
B IR	3582/3598	2.5	3.0	3.5	4±0.4
B IR	3514/3598	3.2	3.7	4.4	4±0.4
B Ra	3514/3582	0.88	1.00	1.11	4±0.4
B Ra	3504/3576	0.22	1.38	4.6	2±0.2
B Ra	3514/3504	5.9	18.0	79	4.5±0.45
B Ra	3582/3576	7.6	14.4	54	2±0.2
B Ra	3514/3594	2.7	3.5	4.7	5±0.5
B Ra	3582/3594	2.8	3.7	4.8	4±0.4
P IR hom	3516/3575	0.73	0.91	1.12	4±0.4
P IR het	3506/3573	0.63	0.89	1.22	4±0.4
P IR het	3575/3597	1.03	1.52	2.3	4±0.4
P IR het	3506/3597	0.88	1.34	2.0	4±0.4
P Ra hom	3516/3575	1.29	1.45	1.63	6±0.6
P Ra hom	3575/3592	2.3	3.4	5.3	6±0.6
P Ra hom	3516/3592	3.2	4.9	7.6	6±0.6
P Ra het	3506/3573	0.80	1.08	1.41	6±0.6
P Ra het	3573/3592	0.69	0.94	1.24	6±0.6
P Ra het	3506/3592	0.74	1.01	1.32	6±0.6

6 Conformational Temperatures

In Figs. S10 to S13 conformational freezing temperatures are visualized for different quantum chemical methods and experiments (IR: filled symbols, Raman: empty symbols) as well as band pairs including different acceptors π (squares) or O (circles) of the respective O^{g}π conformer(s). Error bars only include the integration uncertainty (95% confidence interval from 2.5% and 97.5% quantiles).

Colored backgrounds represent the expected ranges for the conformational freezing temperature for a low-barrier (20–100 K, green) or a high-barrier interconversion (100–330 K, yellow). Values larger than the nozzle temperature (uniformly represented as >330 K, red) are unexpected, as are negative T_c-values (violet), with the latter being equivalent to a wrongly predicted energy sequence. Values between 0 and 20 K (blue) indicate an underestimation of the energy difference.

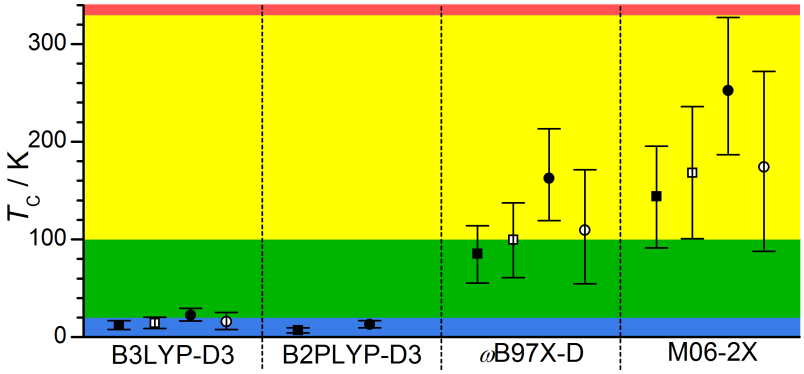

Figure S10: **B** dimer conformational freezing temperatures T_c for the conversion from hetO^{g}π to homO^{g}π.

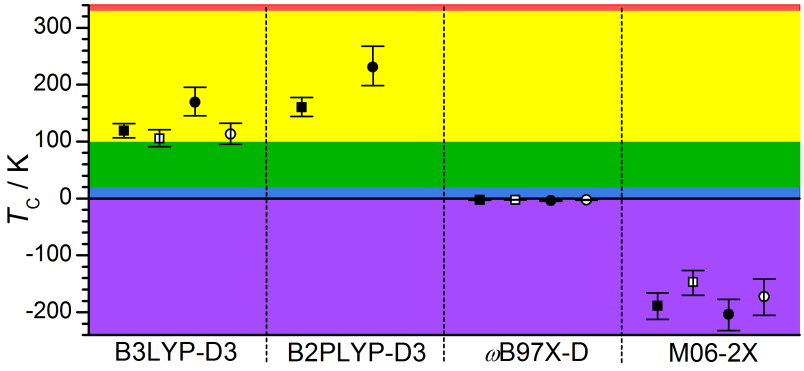

Figure S11: **B** dimer conformational freezing temperatures T_c for the conversion from hetππ to homO^{g}π.

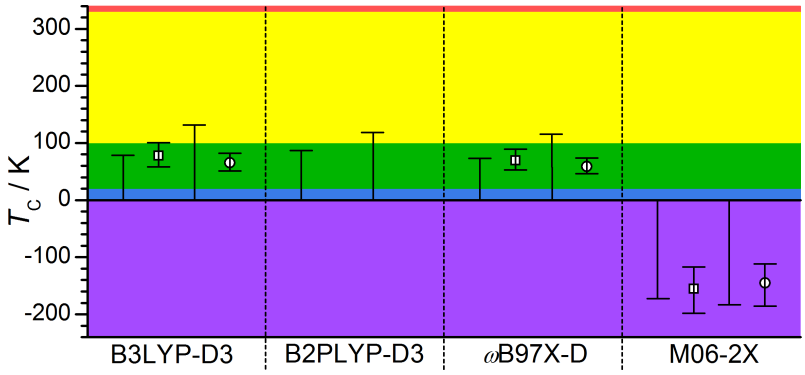

Figure S12: **P** dimer conformational freezing temperatures T_c for the conversion from hom$\pi\pi$ to hom$O^g\pi$. The expected IR-active transition of hom$O^g\pi$ at about 3597 cm^{-1} is not observed in the FTIR-detected expansion, likely due to the higher dilution. Therefore we cannot calculate a mean value for the conformational temperature (absence of filled symbols), but based on the signal-to-noise ratio we can still estimate the upper limit of the 95% confidence interval.[6] The OH$\cdots\pi$ and OH$\cdots$O bands of hom$O^g\pi$ are with a confidence of 97.5% at least 3.9 respectively 3.4 more intense than any potential band below the detection limit.

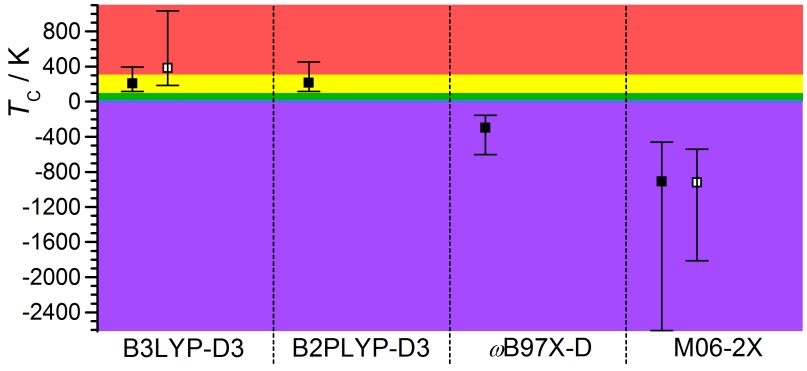

Figure S13: **P** dimer conformational freezing temperatures T_c for the conversion from het$\pi\pi$ to het$O^g\pi$. Due to accidental proximity to the singularity $\lim_{x\to 1\pm}[\ln(x)]^{-1} = \pm\infty$ in Eq. 1 of the main document only very inaccurate values are obtained from the band for the oxygen acceptor (and from the band for the π acceptor with ωB97X-D Raman cross sections), which are omitted.

References

[1] M. J. Frisch, G. W. Trucks, H. B. Schlegel, G. E. Scuseria, M. A. Robb, J. R. Cheeseman, G. Scalmani, V. Barone, B. Mennucci, G. A. Petersson, H. Nakatsuji, M. Caricato, X. Li, H. P. Hratchian, A. F. Izmaylov, J. Bloino, G. Zheng, J. L. Sonnenberg, M. Hada, M. Ehara, K. Toyota, K. Fukuda, J. Hasegawa, M. Ishida, T. Nakajima, Y. Honda, O. Kitao, H. Nakai, T. Vreven, J. A. J. Montgomery, J. E. Peralta, F. Ogliaro, M. Bearpark, J. J. Heyd, E. Brothers, K. N. Kudin, V. N. Staroverov, R. Kobayashi, J. Normand, K. Raghavachari, A. Rendell, J. C. Burant, S. S. Iyengar, J. Tomasi, M. Cossi, N. Rega, J. M. Millam, M. Klene, J. E. Knox, J. B. Cross, V. Bakken, C. Adamo, J. Jaramillo, R. Gomperts, R. E. Stratmann, O. Yazyev, A. J. Austin, R. Cammi, C. Pomelli, J. W. Ochterski, R. L. Martin, K. Morokuma, V. G. Zakrzewski, G. A. Voth, P. Salvador, J. J. Dannenberg, S. Dapprich, A. D. Daniels, Ö. Farkas, J. B. Foresman, J. V. Ortiz, J. Cioslowski and D. J. Fox, *Gaussian 09, Revision E.01*, Gaussian, Inc. technical report, 2009.

[2] N. O. B. Lüttschwager, *Raman Spectroscopy of Conformational Rearrangements at Low Temperatures Folding and Stretching of Alkanes in Supersonic Jets*, Springer International Publishing, Cham, 2014.

[3] M. Gawrilow and M. A. Suhm, *Phys. Chem. Chem. Phys.*, 2020, **22**, 15303–15311.

[4] P. Zielke, *Ramanstreuung am Überschallstrahl: Wasserstoffbrückendynamik aus neuer Perspektive*, Dissertation, Georg-August-Universität Göttingen, 2007.

[5] T. N. Wassermann, *Umgebungseinflüsse auf die C–C- und C–O-Torsionsdynamik in Molekülen und Molekülaggregaten: Schwingungsspektroskopie bei tiefen Temperaturen*, Dissertation, Georg-August-Universität Göttingen, 2010.

[6] G. Karir, N. O. B. Lüttschwager and M. A. Suhm, *Phys. Chem. Chem. Phys.*, 2019, **21**, 7831–7840.